BNL 30202

presented at International Conference on
High Energy Physics, Lisbon, Portugal
July 1981

CONF-810760--6

OG 608

A Comparison of Antiproton-Proton and Proton-Proton Collisions at the CERN Intersecting Storage Ring

A. di Ciaccio, H. Gordon, R. Hogue, T. Killian, T. Ludlam, M. Winik and C. Woody; Brookhaven National Laboratory, Upton, NY 11973

O. Botner, V. Burkert, D. Cockerill, M. Evans, C.W. Fabjan, T. Ferbel, P. Frandsen, A. Hallgren, B. Heck, H.J. Hilke, P. Jeffreys, G. Kesseler, J. Lindsay, J. v.d. Lans, H.J. Lubatti, W. Molzon, B.S. Nielsen, L. Rosselet, E. Rosso, R.H. Schindler, D.W. Wang, Ch. J. Wang, W.J. Willis and W. Witzeling; CERN, Geneva, Switzerland

H. Beggild, E. Dahl-Jensen, I. Dahl-Jensen, P. Dam, G. Damgaard, K.H. Hansen, J. Hooper, E. Lohse, R. Møller, S.Ø. Nielsen, L.H. Olsen and B. Schistad; Niels Bohr Institute, Copenhagen, Denmark

T. Åkesson, S. Almehed, S. Henning, G. Jarlskog, B. Lorstad, A. Melin, U. Mjörnmark and A. Nilsson, University of Lund, Sweden

M.G. Albrow, N.A. McCubbin, Rutherford Laboratory, Chilton, Didcot, U.K.

O. Benary, S. Dagan, D. Lissauer and Y. Oren, University of Tel Aviv, Israel

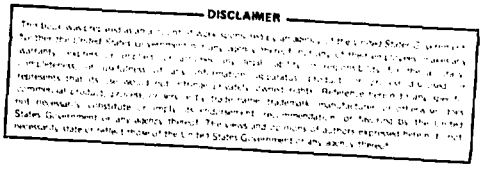

EUROPEAN ORGANIZATION FOR NUCLEAR RESEARCH

CERN/EP
1st July 1981

A COMPARISON OF ANTIPROTON-PROTON AND PROTON-PROTON COLLISIONS AT THE CERN INTERSECTING STORAGE RING

A. di Ciaccio, H. Gordon, R. Hogue, T. Killian, T. Ludlam, M. Winik and C. Woody; Brookhaven National Laboratory, Upton, New York, USA.

O. Botner, V. Burkert, D. Cockerill, M. Evans, C.W. Fabjan, T. Ferbel, P. Frandsen, A. Hallgren, B. Heck, H.J. Hilke, P. Jeffreys, G. Kesseler, J. Lindsay, J. v.d. Lans, H.J. Lubatti, W. Molzon, B.S. Nielsen, L. Rosselet, E. Rosso, R.H. Schindler, D.W. Wang, Ch. J. Wang, W.J. Willis and W. Witzeling; CERN, Geneva, Switzerland.

H. Bøggild, E. Dahl-Jensen, I. Dahl-Jensen, P. Dam, G. Damgaard, K.H. Hansen, J. Hooper, E. Lohse, R. Møller, S.Ø. Nielsen, L.H. Olsen and B. Schistad. Niels Bohr Institute, Copenhagen, Denmark.

T. Åkesson, S. Almehed, S. Henning, G. Jarlskog, B. Lörstad, A. Melin, U. Mjörnmark and A. Nilsson, University of Lund, Sweden.

M.G. Albrow, N.A. McCubbin, Rutherford Laboratory, Chilton, Didcot, U.K.

O. Benary, S. Dagan, D. Lissauer and Y. Oren, University of Tel Aviv, Israel.

ABSTRACT

We report on a comparative investigation of $\bar{p}p$ and pp collisions at the CERN Intersecting Storage Rings. The study was performed using the cylindrical drift chamber of the Axial Field Spectrometer. Non-relativistic particles were identified through multiple ionization sampling. We compare the inclusive production of pions, kaons, protons and antiprotons in the central region of rapidity ($|y| < 0.8$). Distributions in charged particle multiplicity, rapidity and p_T are found to be very similar in $\bar{p}p$ and pp data.

Contribution to the International Conference on High Energy Physics, Lisbon, July 1981.

TÅ/mm

1. APPARATUS

The data for this analysis were taken at the CERN Intersecting Storage Rings using the Axial Field Spectrometer (AFS) Fig. 1.

This spectrometer is designed for the investigation of highly inelastic pp collisions. It consists of a cylindrical drift chamber as vertex detector; the drift chamber operates in a 0.5 Tesla axial magnetic field. There is a Cerenkov arm on one side that covers $|y| < 1.0$ and 40° in azimuth. On the side opposite to the Cerenkov arm are two liquid-argon electromagnetic calorimeters. At a later stage of the experiment the vertex detector will be surrounded entirely by a (uranium-scintillator-sandwich) electromagnetic and hadronic calorimeter.

The only parts of the spectrometer used in the present analysis are the drift chamber (Fig. 2) and a barrel hodoscope that surrounds the beam pipe. The vertex detector is a 1.4 m long drift chamber of the "bicycle wheel" configuration with 4° azimuthal segmentation. Each 4° sector contains 42 resistive sense wires (arranged radially into three crowns), that provide non-projective point reconstruction in the transverse plane from drift time and longitudinally from charge division measurement. In addition, multiple ionization sampling (dE/dx) is used for particle identification. Fig. 3 shows the truncated mean of the ionization samples versus the logarithm of the momentum; clear π, K and p discrimination can be observed in the scatter-plot.

The resolution in the chamber is $\sigma = 230$ μm (rms) in drift distance and $\sigma = 1.5$ cm (rms) in the axial coordinate. The truncated mean (for > 30 pulse height measurements) for minimum ionizing tracks has σ(rms)/mean = 11%. The drift chamber is described in more detail in Ref. [1].

2. THE DATA SAMPLES

The data described here consist of 25 000 $\bar{p}p$ events and 36 000 pp events at $\sqrt{s} = 53$ GeV. Both samples were obtained in ISR runs with low luminosity, spaced closely in time, and analyzed with the same set of analysis programs. The trigger used was a minimum bias trigger, defined by a coincidence between scintillation counters surrounding the two beam tubes downstream of the inter-

section region. This trigger is sensitive to about 60% of the inelastic collisions.

3. RESULTS

3.1. p_T Spectra

The p_T spectrum observed for charged particles emitted in pp collisions within the rapidity range $|y| < 0.8$ is shown in Fig. 4, together with the spectrum at 90° measured in previous experiments (Refs [2,3,4]). The two sets of data agree reasonably well in shape of the spectra. There is an uncertainty in normalization of about 10% in both distributions (the rapidity range $|y| < 0.8$ is chosen because the acceptance is almost uniform and close to 100% in this region). This result is compared with the corresponding one from $\bar{p}p$ collisions in Fig. 5, where we plot the ratio of the two spectra. No significant difference is observed.

In limited ranges of momentum we can distinguish $\pi^{\pm}$, $K^{\pm}$ and $p^{\pm}$ from the measurement of dE/dx in the drift chamber. Protons and antiprotons are identified in a region p^{lab} = 200 MeV/c to 800 MeV/c and K mesons in a region p^{lab} = 100 MeV/c to 500 MeV/c. The ratio of the p_T spectra of K mesons from $\bar{p}p$ and pp collisions is given in Fig. 6. There are 12 ± 7% more K^- and 12 ± 7% less K^+ emitted into our region from $\bar{p}p$ collisions than from pp collisions. These differences should be held together with the K^+/K^- ratio in pp collisions. At 90° and at low p_T the K^+ to K^- ratio has previously been measured to be 1.18 ± 0.06 (Ref. [4]) and in this experiment we find 1.24 ± 0.07. The deviation from 1.00 is presumably due to the contribution to the K meson flux at 90° from (K^+, Y) associated production adding to the pair production of K mesons. When one of the proton beams is exchanged with an antiproton beam, we would expect - if the pair production is the same - a ∿ 10% decrease of K^+ and a ∿ 10% increase of K^-, which is close to the observed changes. Since the sum of K^+ and K^- is almost unchanged, there cannot be a large difference in pair production in $\bar{p}p$ and in pp collisions.

Fig. 7 shows ratios similar to those in Fig. 6, but for protons and antiprotons. Here we observe a decrease of (8 ± 5)% in the number of

protons and an increase of (24 ± 6)% in the number of antiprotons produced in the $\bar{p}p$ collisions as compared to pp collisions. There is an indication of a variation with p_T of this production ratio, suggesting a larger effect at higher p_T.

3.2. Rapidity Distributions

The rapidity distributions of all charged particles in the two data samples are compared in Fig. 8; positive and negative particles are shown separately in Fig. 9, and particles with $p_T > 1.0$ GeV/c in Fig. 10 in order to see if we can trace the directions of the incoming charges (the antiproton beam is in the direction of negative rapidity). The ratios of the observed rapidity distributions show no variation with y. Averaged over rapidity we see 3.8 ± 0.7% fewer positive particles and 2.8 ± 0.7% more negative particles in $\bar{p}p$ collisions than in pp collisions. For $K^{\pm}$ p and $\bar{p}$ the ratios of the rapidity distributions are plotted separately in Figs. 11 and 12. With the present statistics no clear variation can be seen with y. On the other hand the changes in the distributions of final state protons and antiprotons from $\bar{p}p$ to pp collisions must depend on rapidity since at least a part of them is the change in the scattering of beam particles into our region. The y dependence to be expected of the production ratios for protons and antiprotons can be estimated from the known cross sections for $pp \to p + X$ and $pp \to \bar{p} + X$ [4], assuming that pair creation of protons and antiprotons is the same in $\bar{p}p$ as in pp collisions. The estimate involves an evaluation of the distribution of protons in pp collisions that originate from one of the beams. Fig. 13 illustrates this evaluation for protons with $p_T = 0.6$ GeV/c giving the production ratios as sketched in Figs. 11 and 12. There is reasonable agreement with the observed ratios.

3.3. Charged Particle Multiplicity Distributions

The charged particle multiplicity distributions in the two data samples are shown in Fig. 14, and the ratio between them plotted in Fig. 15. The $\bar{p}p$ collisions seem to populate the high multiplicity tail more strongly than the pp collisions. Such an effect could be connected with the small fraction of annihilation events in the $\bar{p}p$ collisions. From an extrapolation of the difference in the $\bar{p}p$ and pp total cross sections ($\Delta\sigma$) measured as a

function of $\sqrt{s}$ at lower energies [5], we find that at $\sqrt{s}$ = 53 GeV, $\Delta\sigma$ = 0.9 mb or 2.6% of σ_{inel}. A fraction of this magnitude of the $\bar{p}p$ collisions might provide a special class of final states, for example with high multiplicities. In our region of rapidity the pp collisions have $\langle n \rangle$ = 2.7. Maybe the observed effect can be understood as coming from 2.6% of the $\bar{p}p$ collisions having $\langle n \rangle = 2.7 + \varepsilon$ and a scaled multiplicity distribution around this higher $\langle n \rangle$. The ratio between a composed distribution and a distribution with $\langle n \rangle$ = 2.7 is drawn on Fig. 15 for ε = 1, 2 and 3. The observations are well described by $\varepsilon = 1.7 \pm 1.0$ i.e. an increase of the order of 60% of $\langle n \rangle$ in the central region for the annihilations. However at the present level of precision ε could also be zero.

4. BACKGROUND ESTIMATE

To estimate the background produced by beam gas and beam pipe interactions, we took data with only the proton beam present. In 36 minutes we got 256 triggers of which two were accepted as events by the offline analysis program. From this we can estimate that less than seven events in a thousand are background events in the $\bar{p}p$ data sample. Systematic effects might might arise from small variations in the run conditions and program inefficiencies are not included in the errors given.

5. CONCLUSIONS

Within the limited analysis power represented by the available antiproton sample of 25,000 Minimum Bias triggered events we have compared the production of particles in $\bar{p}p$ and pp collisions at $\sqrt{s}$ = 53 GeV in the rapidity range $|y| < 0.8$ and in the p_T range up to 1.5 GeV/c. We found that $\bar{p}p$ and pp collisions are similar within errors except for such changes in charge and baryon number flow, which can be understood as consequences of the change in quantum numbers of one of the colliding particles. In particular we have not observed any increase of the pair production of $K^{\pm}$ or $p^{\pm}$ in $\bar{p}p$ collisions. An indication is observed that a small fraction (the annihilation part) of the $\bar{p}p$ collisions lead to higher charge multiplicity in the central region than the bulk of $\bar{p}p$ collisions, which are similar to pp collisions.

This research supported in part by the U.S. Department of Energy.

REFERENCES

1 D. Cockerill et al., NIM 176 (1980) 159-162.

2 K. Guettler et al., Nucl. Phys. B116 (1976) 77.

3 K. Guettler et al., Phys. Lett. 64B (1976) 111.

4 B. Alper et al., Nucl. Phys. B100 (1975) 237.

5 U. Amaldi et al., Ann. Rev. Nucl. Sc. 26 (1976) 385.

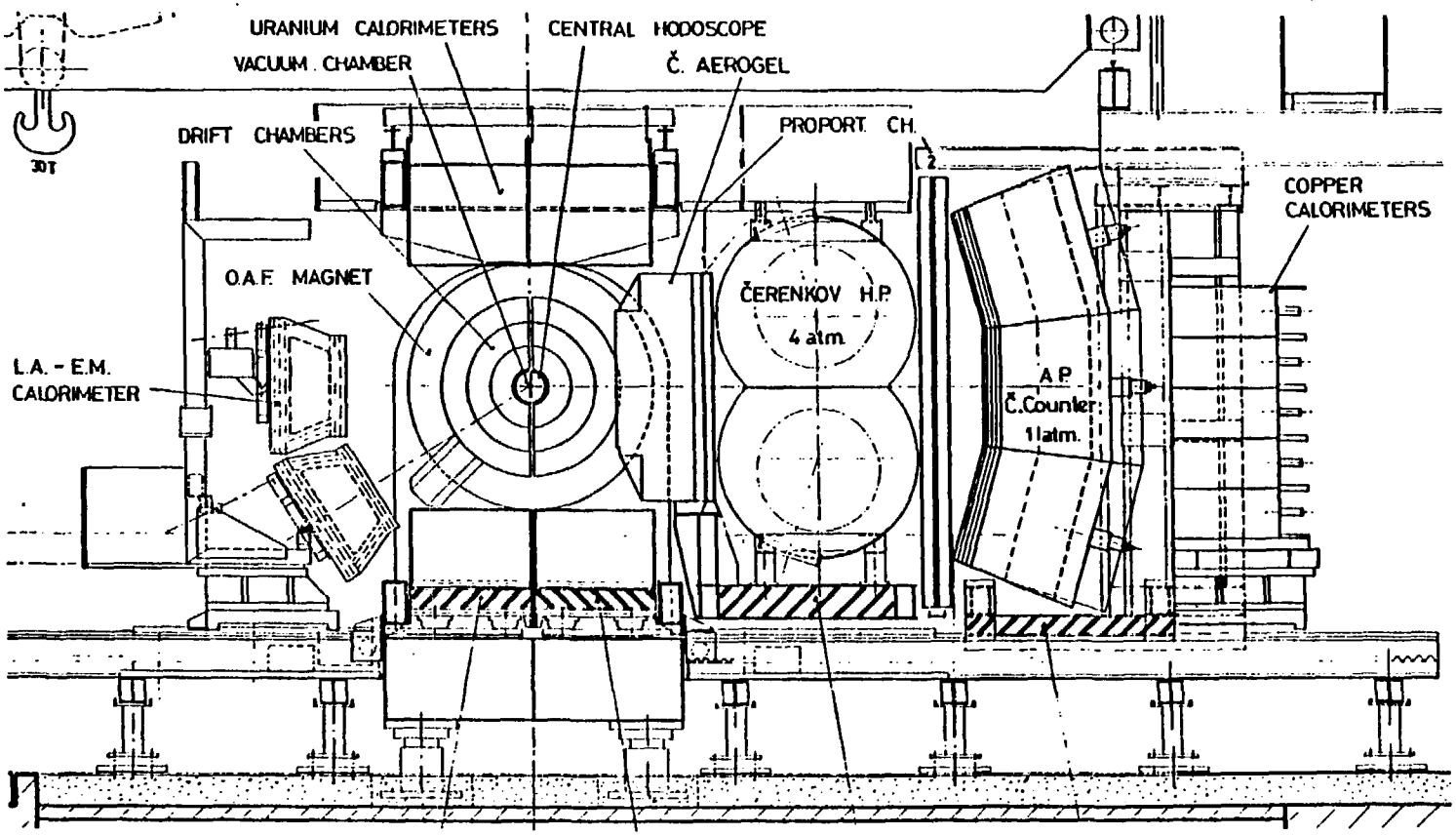

Cross-section through the AFS (1981 configuration). The top and bottom U calorimeters (4 sr total) are being installed during the first half of 1981.

FIGURE 1

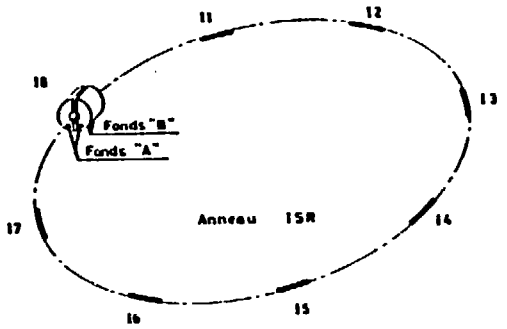

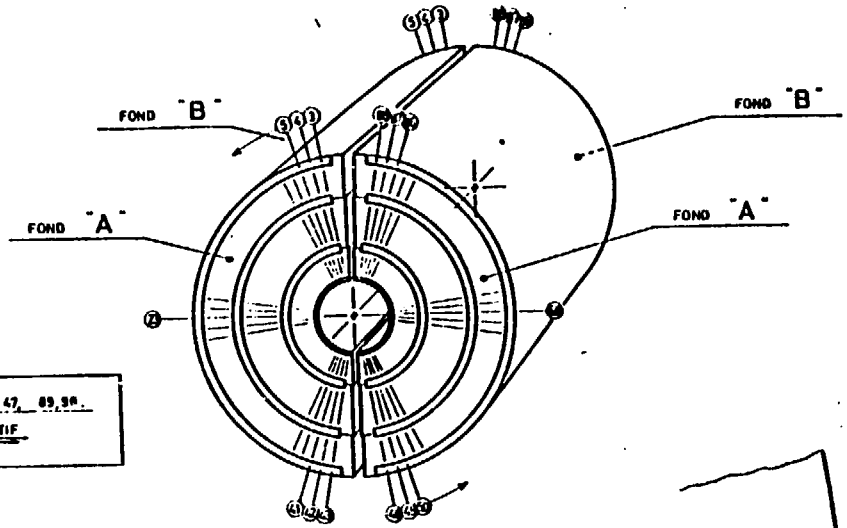

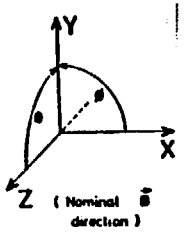

Secteurs = 1,2, 44,45,46,47, 89,90.
NON ACTIF

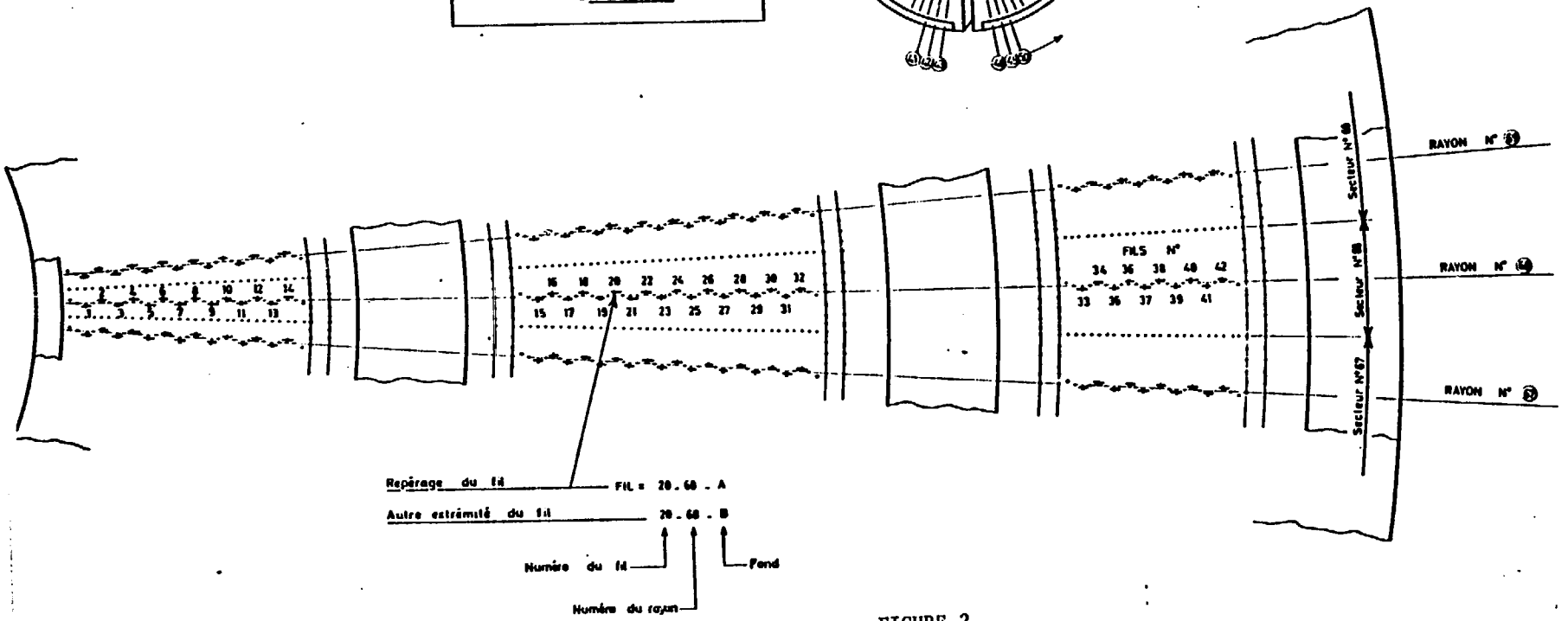

FIGURE 2

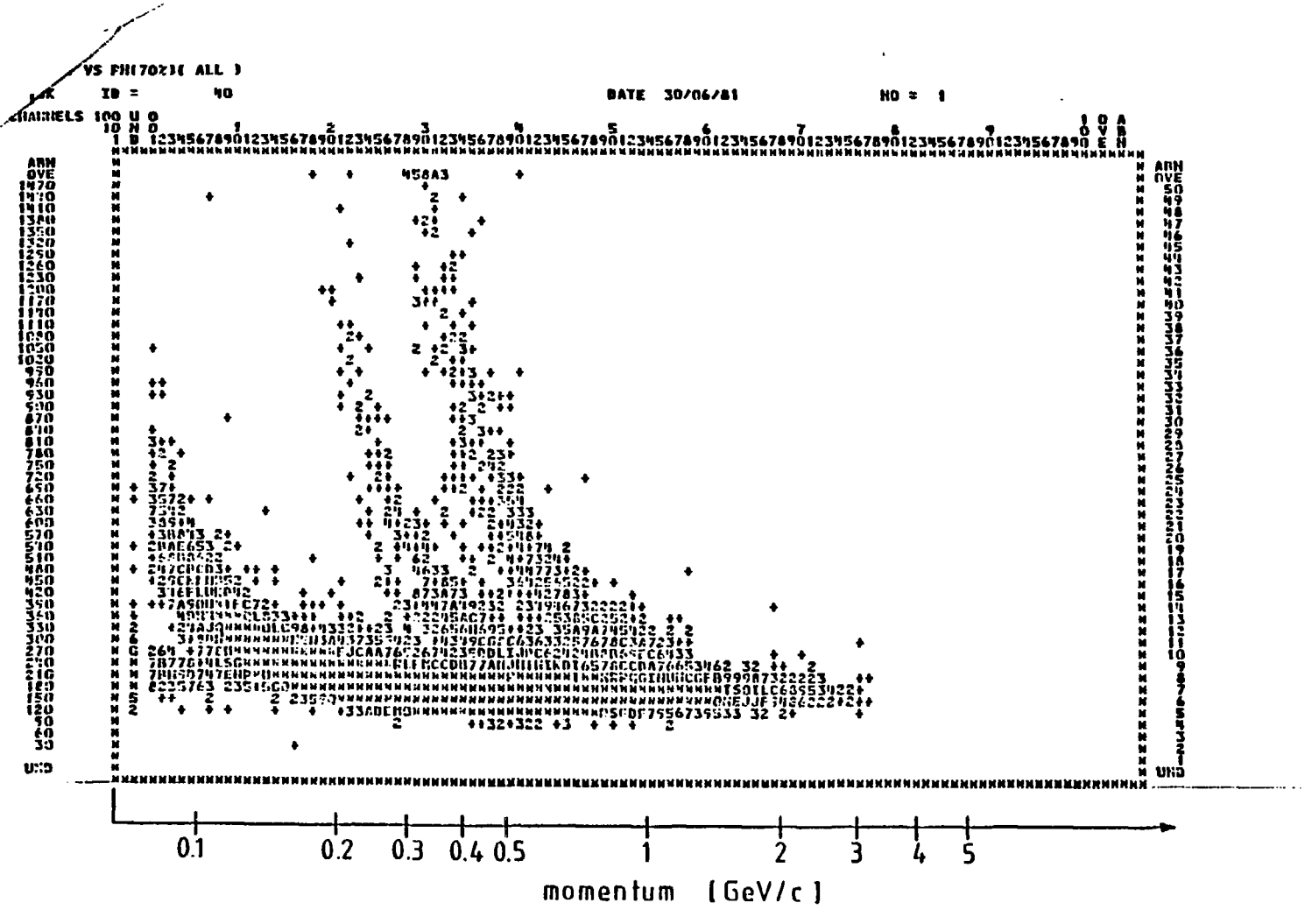

FIGURE 3

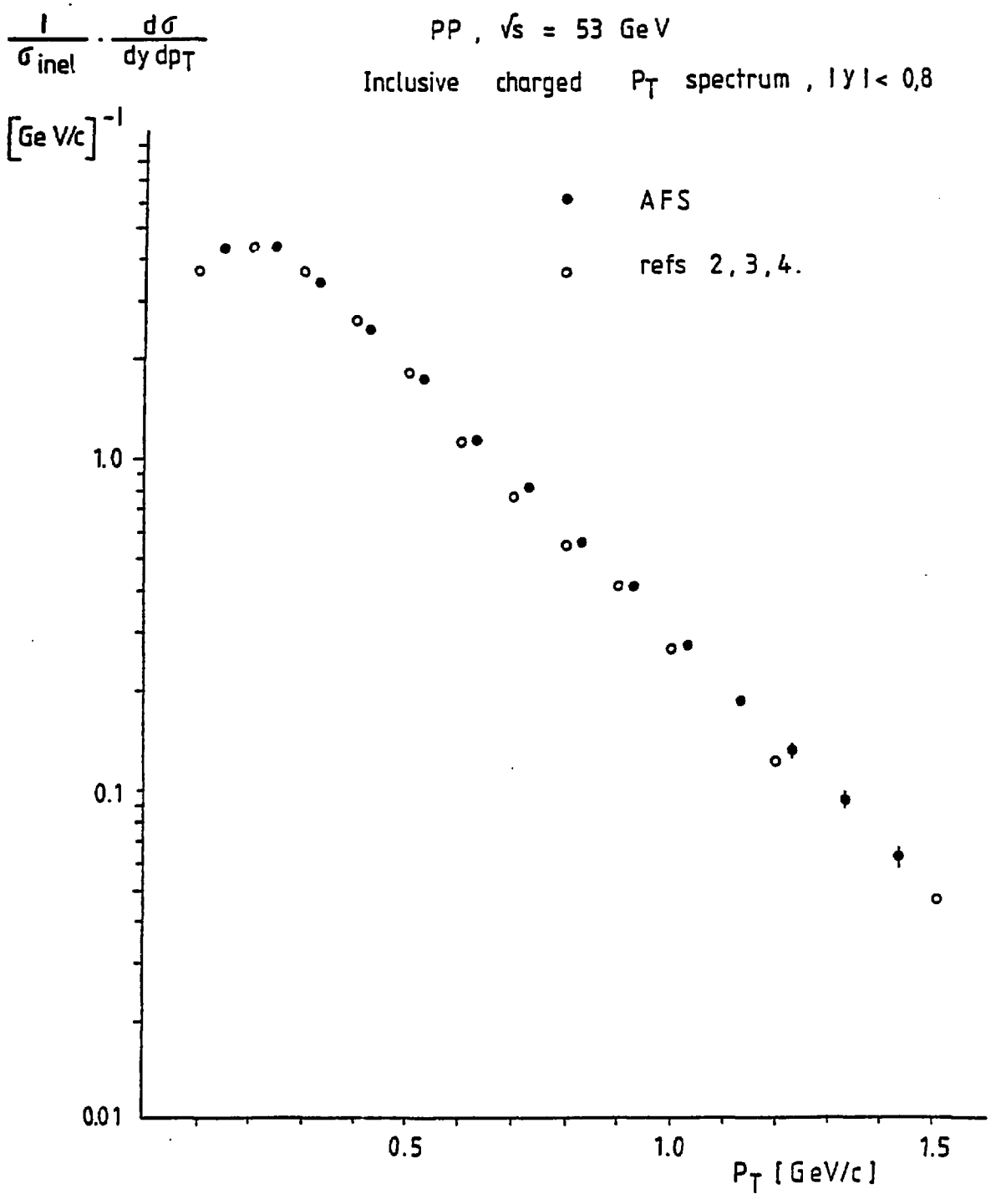
$\frac{1}{\sigma_{inel}} \cdot \frac{d\sigma}{dy\, dp_T}$
PP , $\sqrt{s}$ = 53 GeV
Inclusive charged P_T spectrum , $|y| < 0{,}8$
$[GeV/c]^{-1}$
AFS
refs 2, 3, 4.
1.0
0.1
0.01
0.5
1.0
1.5
P_T [GeV/c]

FIGURE 4

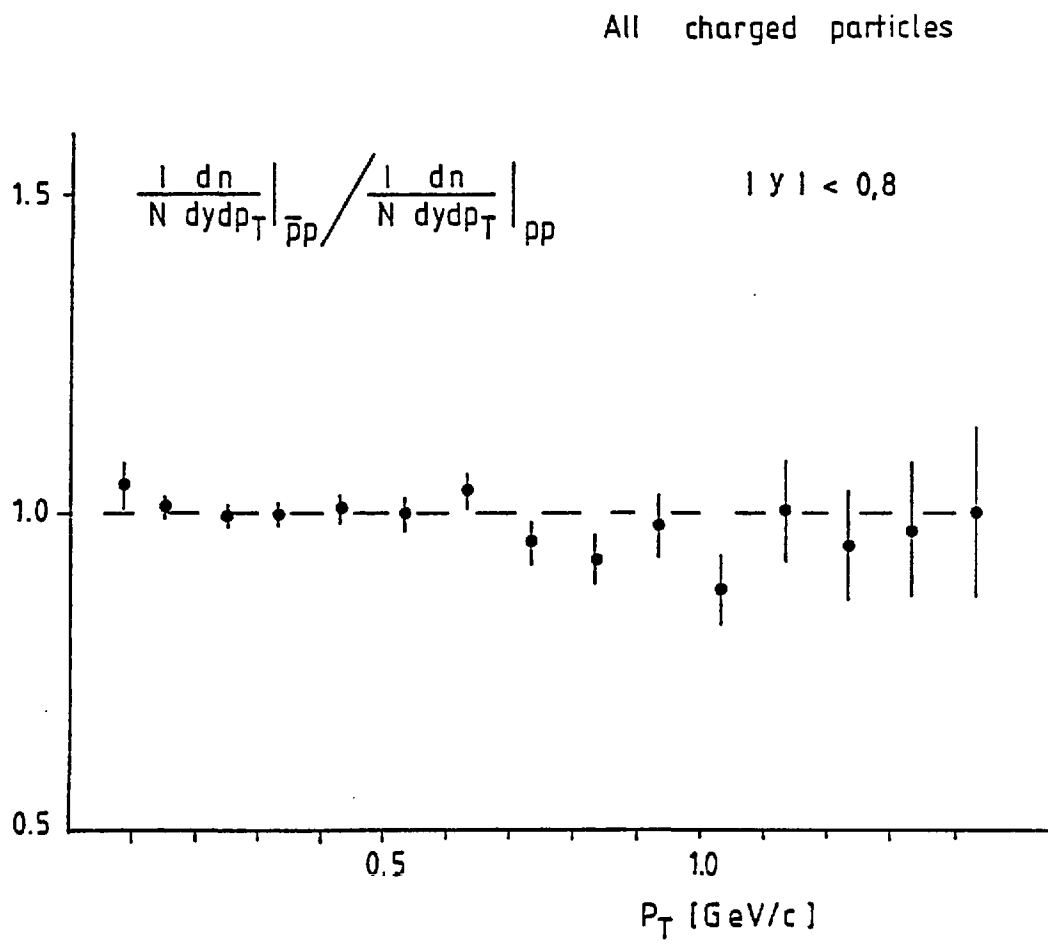
All charged particles
$\frac{1}{N}\frac{dn}{dydp_T}\Big|_{\bar{p}p} \Big/ \frac{1}{N}\frac{dn}{dydp_T}\Big|_{pp}$
| y | < 0,8
1.5
1.0
0.5
0.5
1.0
P_T [GeV/c]

FIGURE 5

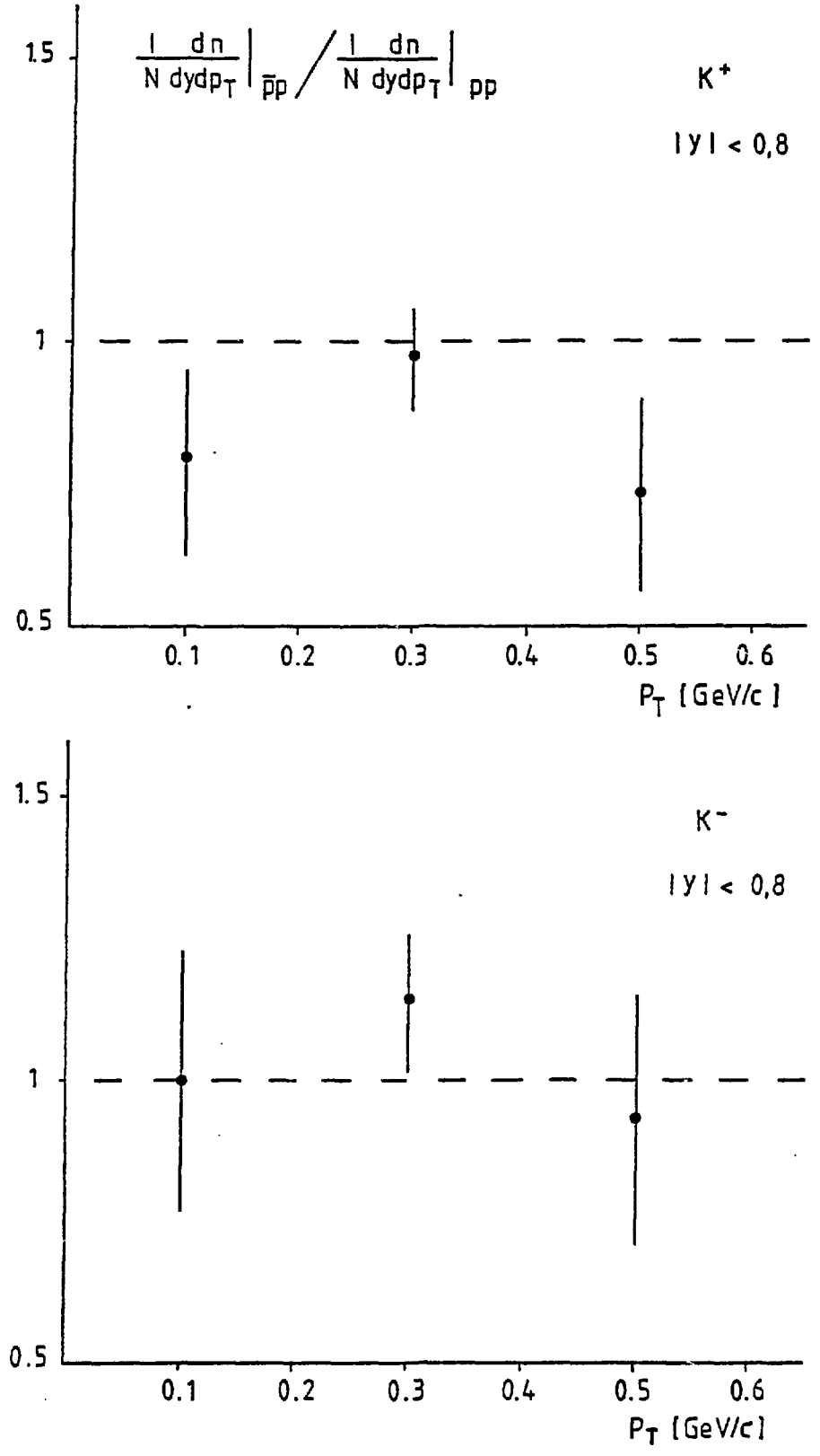
1.5
1
0.5
$\frac{1}{N}\frac{dn}{dydp_T}\Big|_{\bar{p}p} \Big/ \frac{1}{N}\frac{dn}{dydp_T}\Big|_{pp}$
K^+
$|y| < 0,8$
0.1
0.2
0.3
0.4
0.5
0.6
P_T [GeV/c]
1.5
1
0.5
K^-
$|y| < 0,8$
0.1
0.2
0.3
0.4
0.5
0.6
P_T [GeV/c]

FIGURE 6

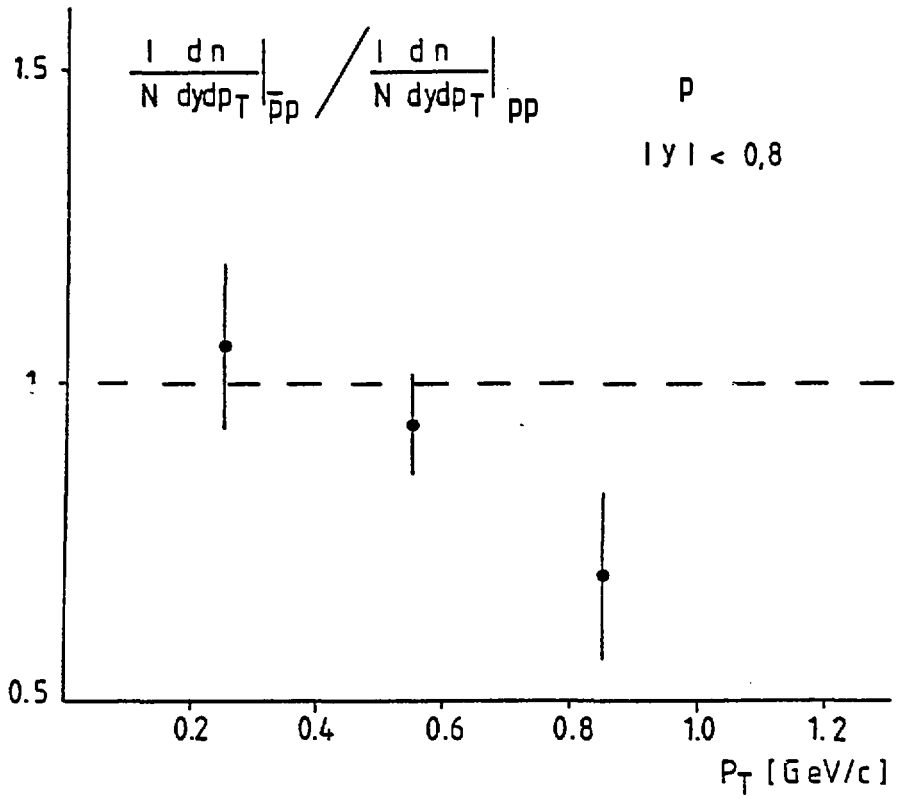
1.5
1
0.5
$\frac{1}{N}\frac{dn}{dydp_T}\Big|_{\bar{p}p} \Big/ \frac{1}{N}\frac{dn}{dydp_T}\Big|_{pp}$
p
|y| < 0,8
0.2
0.4
0.6
0.8
1.0
1.2
P_T [GeV/c]

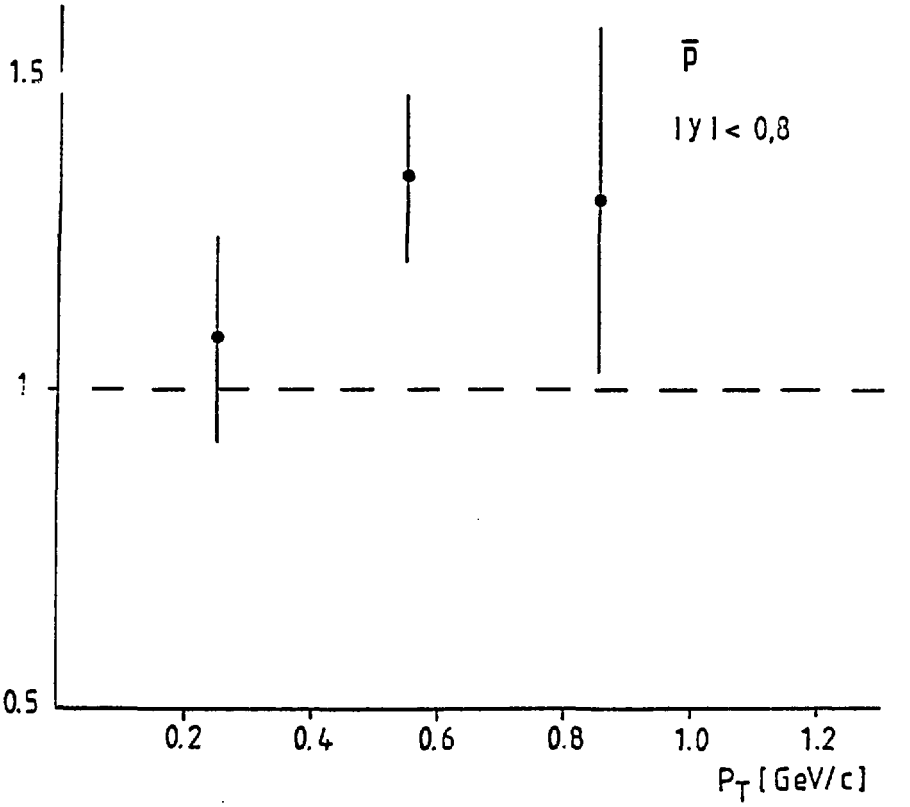
1.5
1
0.5
$\bar{p}$
|y| < 0,8
0.2
0.4
0.6
0.8
1.0
1.2
P_T [GeV/c]

FIGURE 7

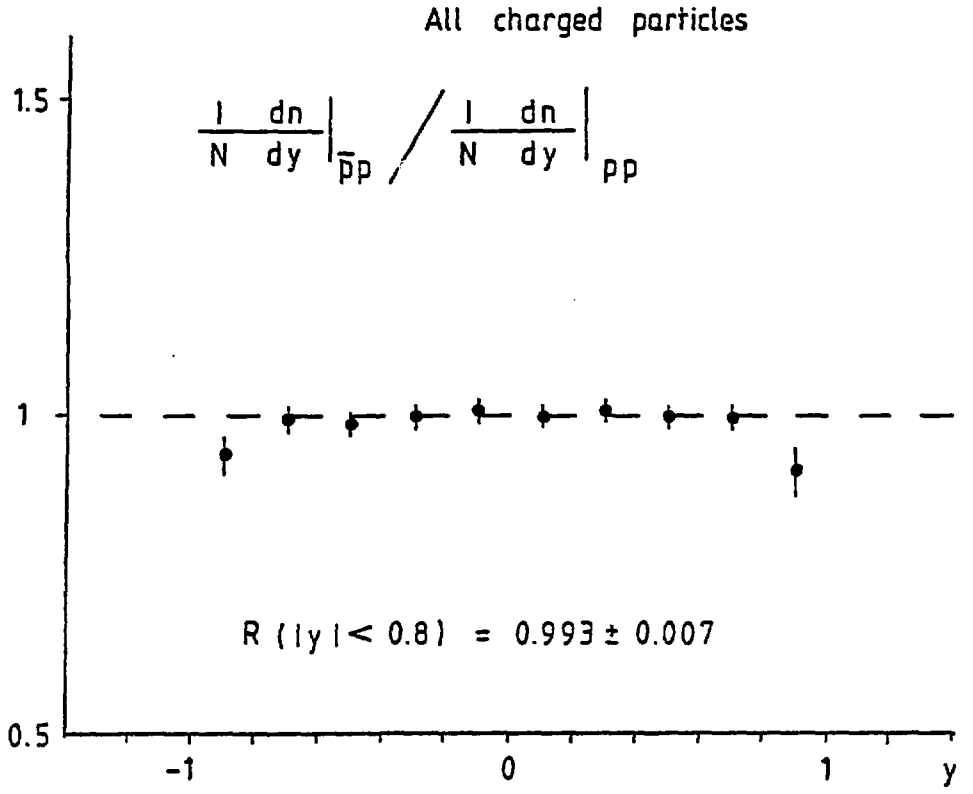
All charged particles
1.5
1
0.5
$\frac{1}{N}\frac{dn}{dy}\Big|_{\bar{p}p} \Big/ \frac{1}{N}\frac{dn}{dy}\Big|_{pp}$
R (|y| < 0.8) = 0.993 ± 0.007
-1
0
1
y

FIGURE 8

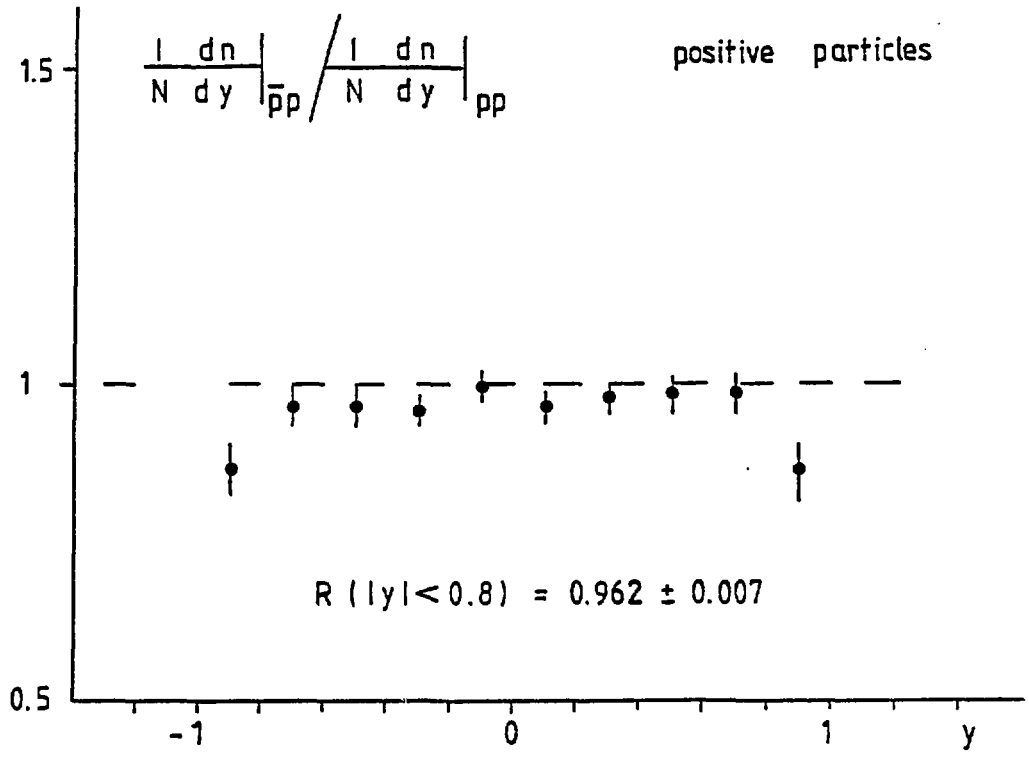
positive particles
1.5
1
0.5
R (|y|< 0.8) = 0.962 ± 0.007
-1
0
1
y

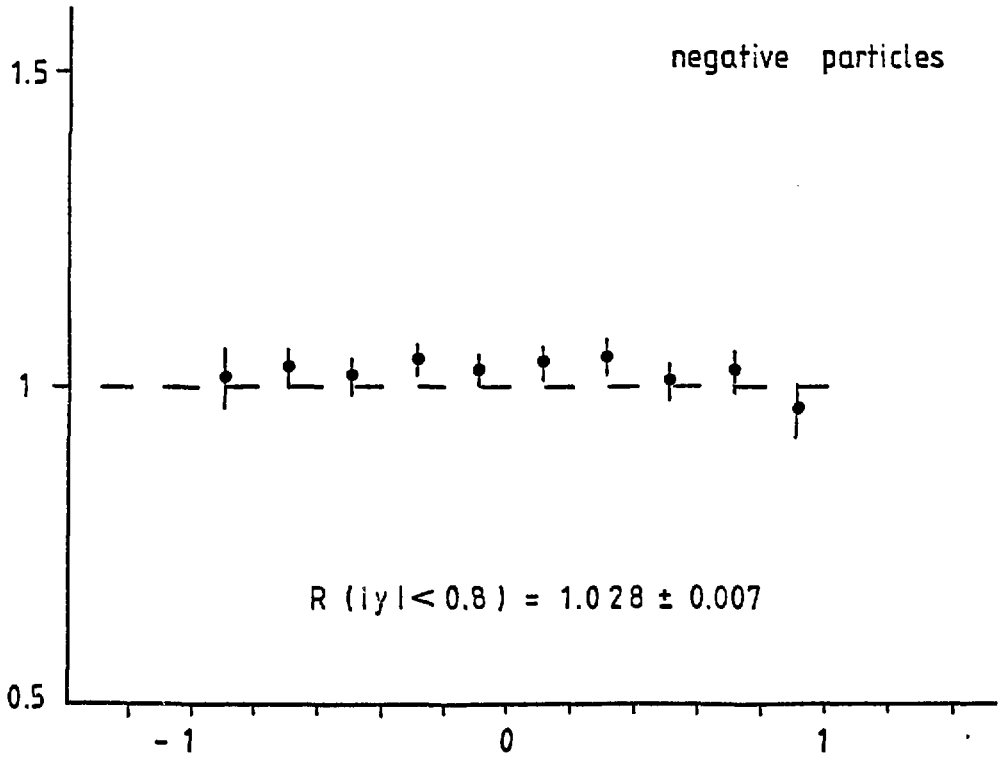
negative particles
1.5
1
0.5
R (|y|< 0.8) = 1.028 ± 0.007
-1
0
1

FIGURE 9

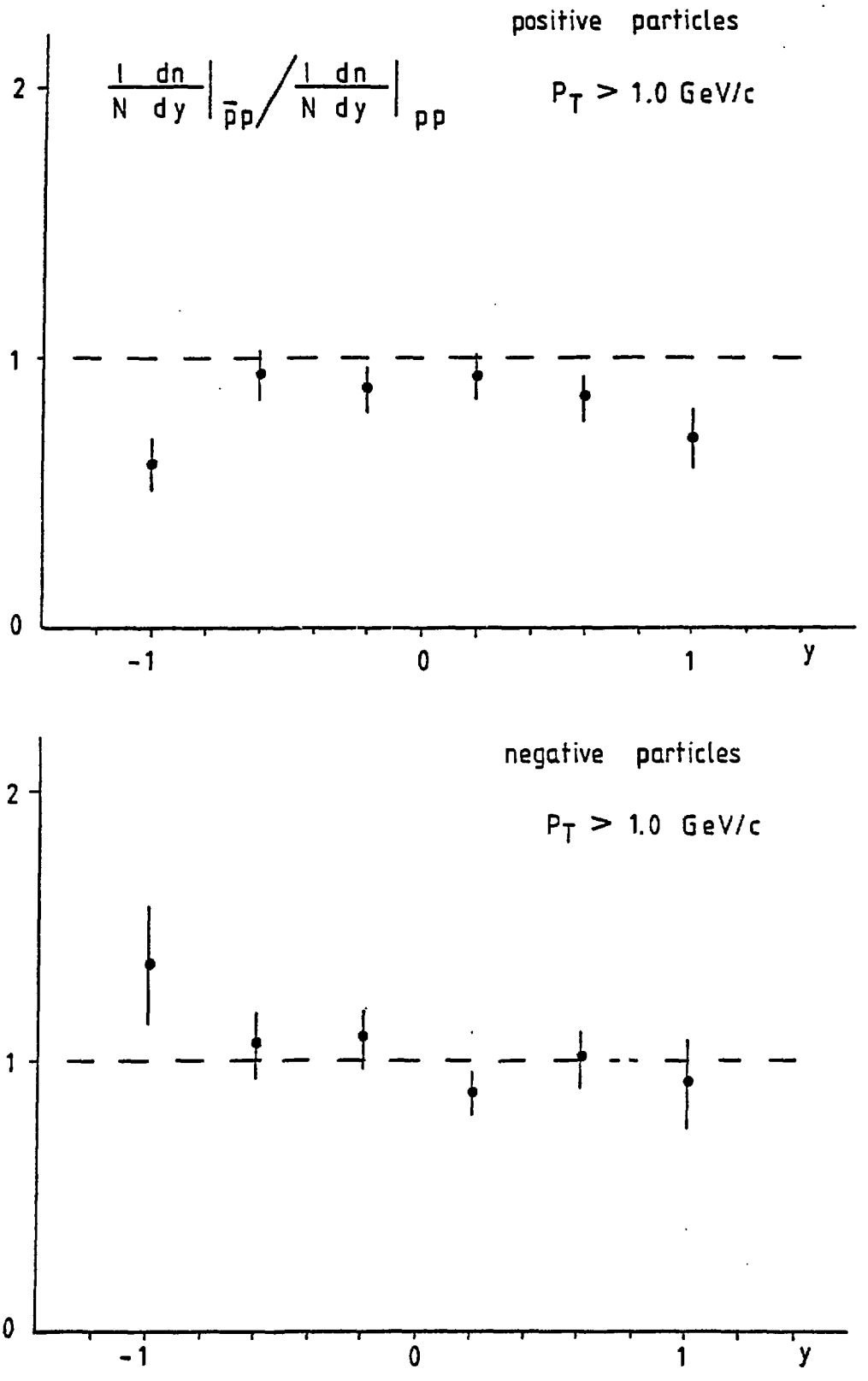
positive particles
$\frac{1}{N}\frac{dn}{dy}\Big|_{\bar{p}p} \Big/ \frac{1}{N}\frac{dn}{dy}\Big|_{pp}$
$P_T > 1.0$ GeV/c
2
1
0
-1
0
1
y
negative particles
$P_T > 1.0$ GeV/c
2
1
0
-1
0
1
y

FIGURE 10

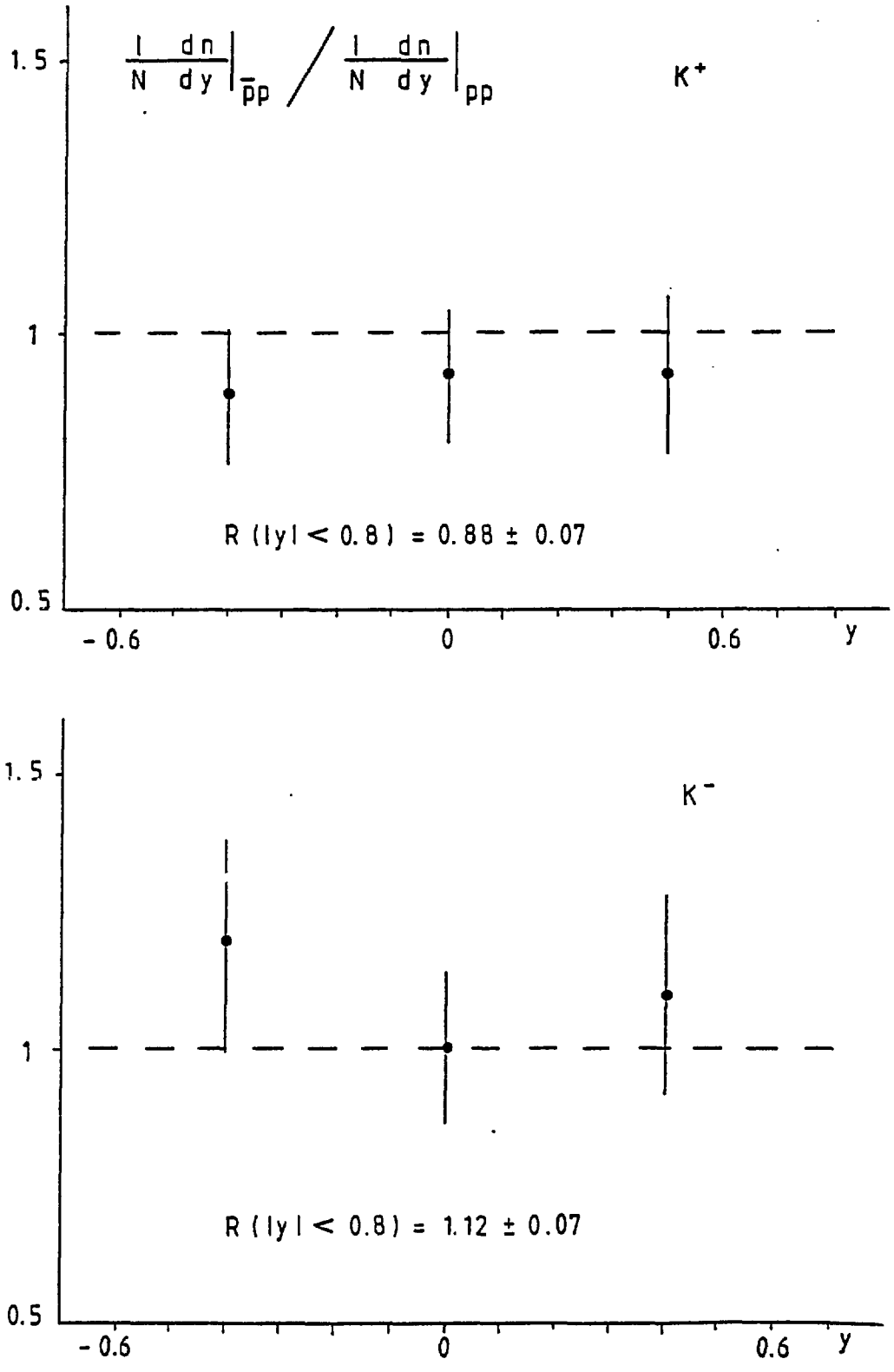
1.5
1
0.5
$\frac{1}{N}\frac{dn}{dy}\Big|_{\bar{p}p} \Big/ \frac{1}{N}\frac{dn}{dy}\Big|_{pp}$
K^+
R (|y| < 0.8) = 0.88 ± 0.07
- 0.6
0
0.6
y
1.5
1
0.5
K^-
R (|y| < 0.8) = 1.12 ± 0.07
- 0.6
0
0.6
y

FIGURE 11

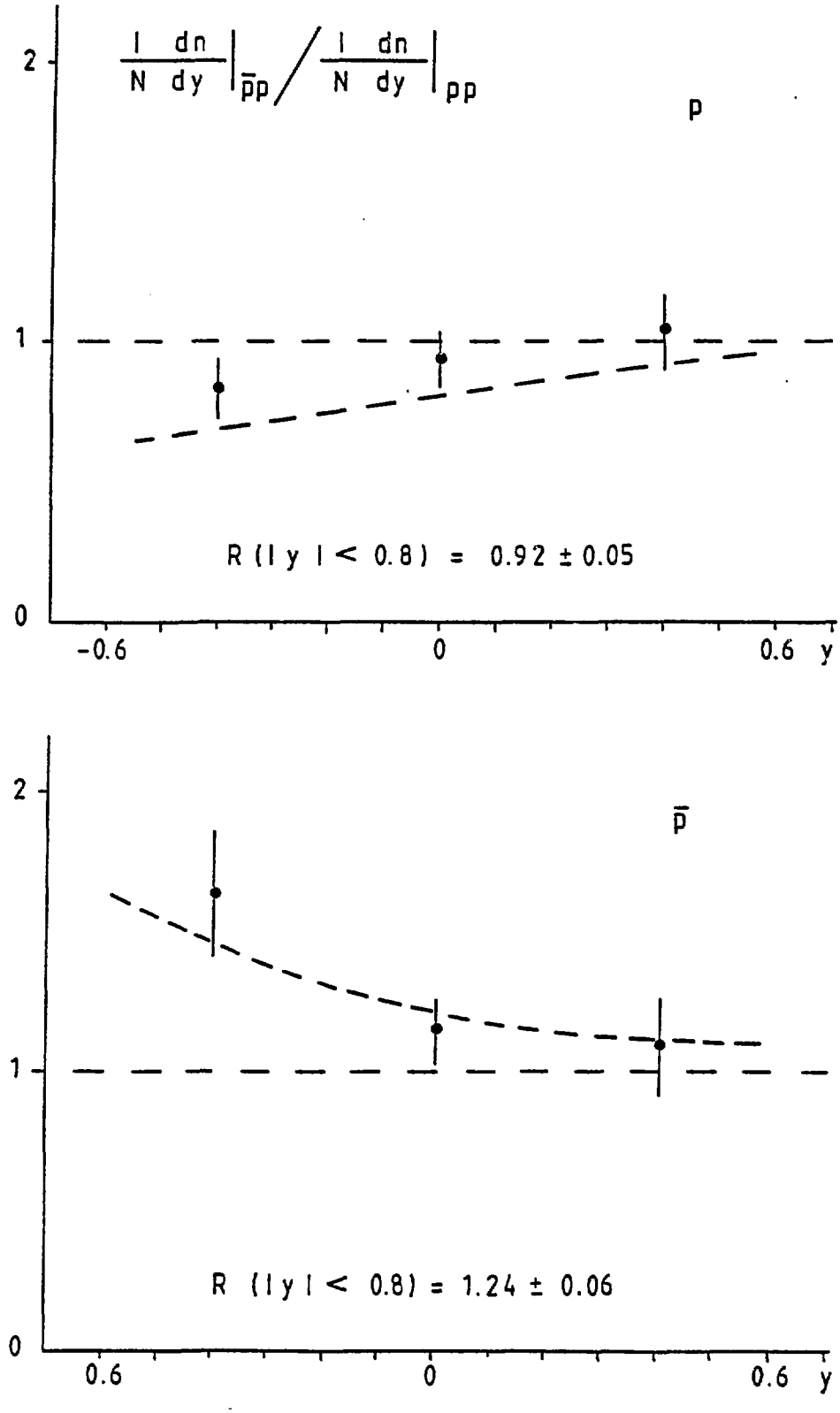
$\frac{1}{N}\frac{dn}{dy}\Big|_{\bar{p}p} \Big/ \frac{1}{N}\frac{dn}{dy}\Big|_{pp}$
p
2
1
0
R (| y | < 0.8) = 0.92 ± 0.05
-0.6
0
0.6
y
$\bar{p}$
2
1
0
R (| y | < 0.8) = 1.24 ± 0.06
0.6
0
0.6
y

FIGURE 12

FIGURE 13

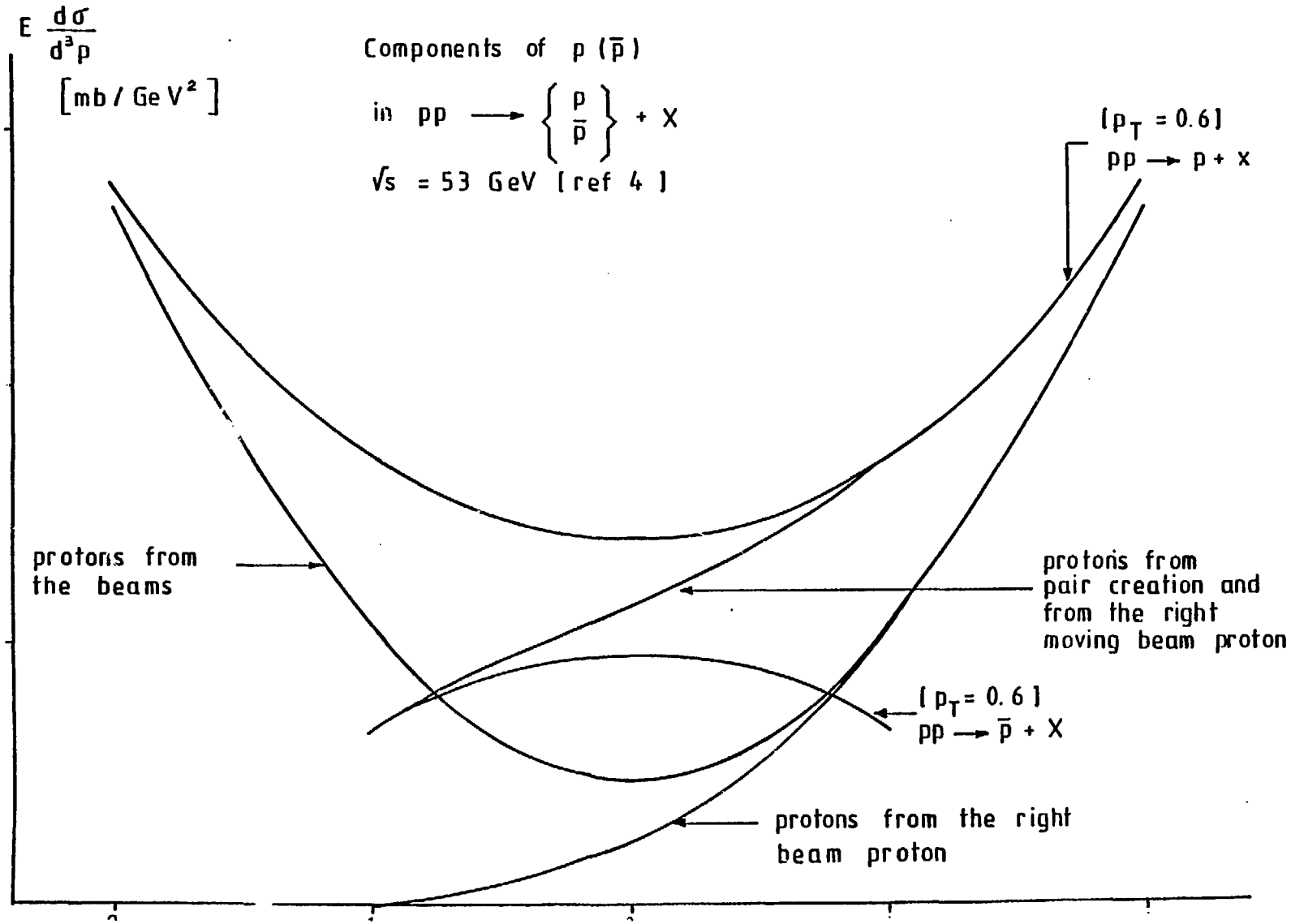
E dσ/d³p
[mb / GeV²]
Components of p (p̄)
in pp → { p, p̄ } + X
√s = 53 GeV [ref 4]
1.5
1
0.5
[p_T = 0.6]
pp → p + x
protons from the beams
protons from pair creation and from the right moving beam proton
[p_T = 0.6]
pp → p̄ + X
protons from the right beam proton

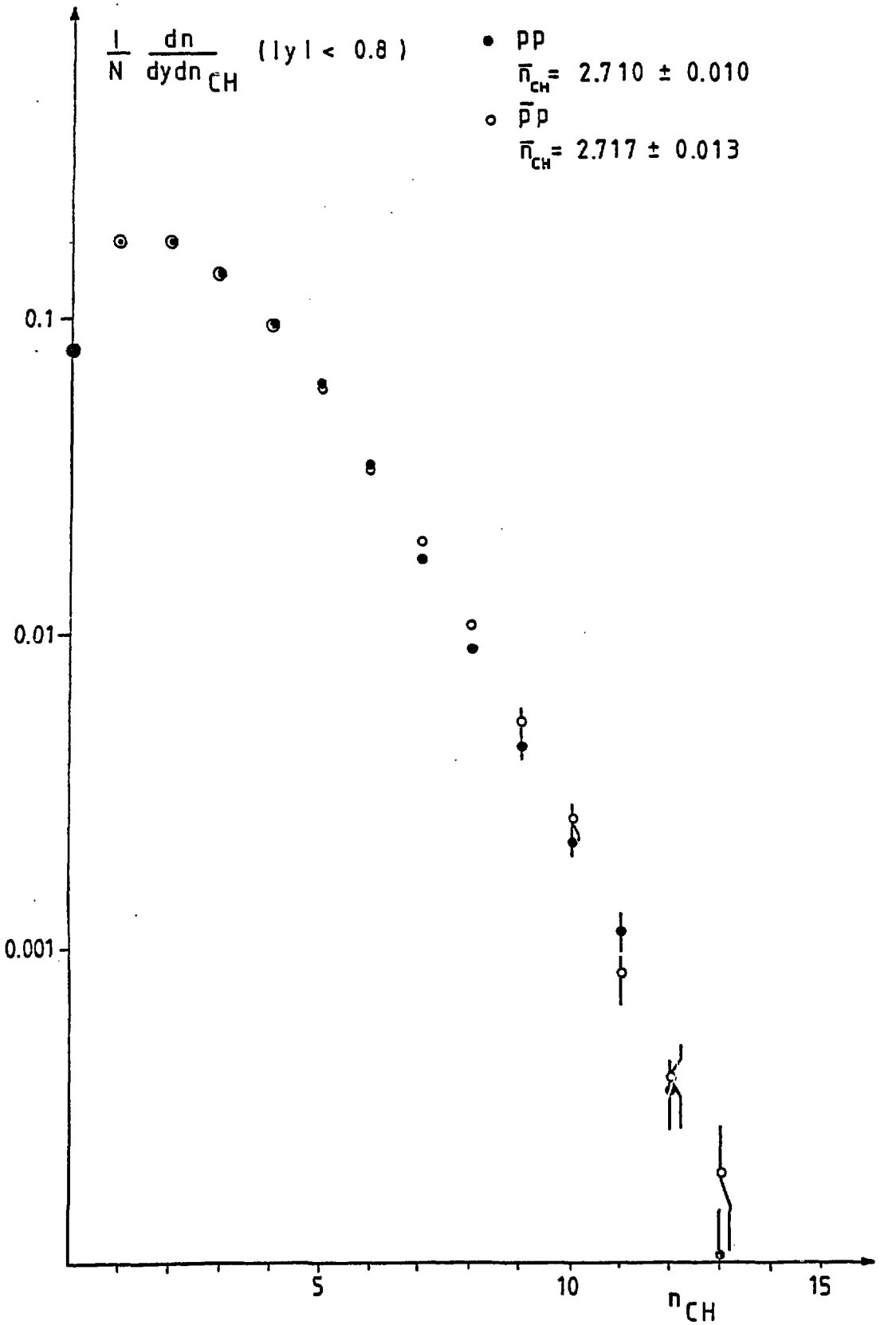
$\frac{1}{N}\frac{dn}{dydn_{CH}}$ (|y| < 0.8)
pp
$\bar{n}_{CH}$ = 2.710 ± 0.010
$\bar{p}p$
$\bar{n}_{CH}$ = 2.717 ± 0.013
0.1
0.01
0.001
5
10
15
n_{CH}

FIGURE 14

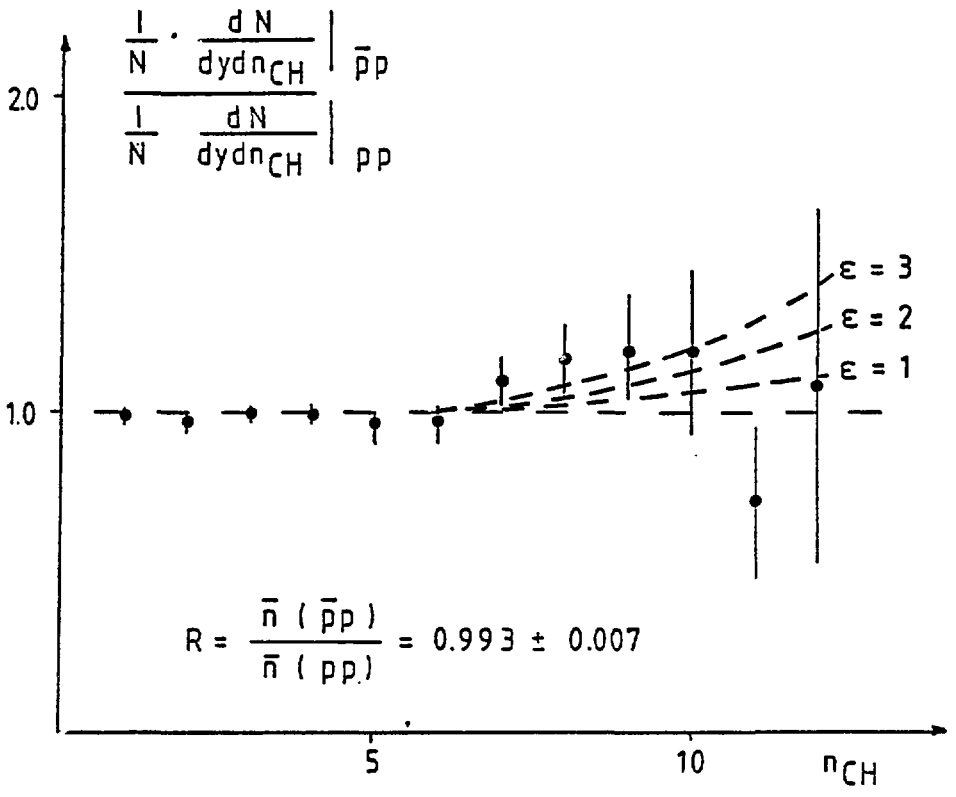

$\Delta\sigma = \sigma_{tot}(p\bar{p}) - \sigma_{tot}(pp) = 0.9$ mb
at $\sqrt{s} = 53$ GeV

i.e. 2.6 % of σ inelastic (pp)

$\langle n_{CH} \rangle = 2.7$ in pp

$$R = \frac{Fn(2.7) + 0.026\, Fn(2.7+\varepsilon)}{1.026 \times Fn(2.7)}$$

Fn = multiplicity distribution

FIGURE 15